Author Manuscript

Authors: Lu Li; Yichen Wang; Srinivas Vanka; Xiaoyue Mu; Zetian Mi; Chao-Jun Li

Nitrogen Photofixation over III-Nitride Nanowires Assisted by Ruthenium Clusters of Low Atomicity

Lu Li, Yichen Wang, Srinivas Vanka, Xiaoyue Mu, Zetian Mi[*] and Chao-Jun Li[*]

Abstract: In many heterogeneous catalysts, the interaction of supported metal species with matrix can alter the electronic and morphological properties of metal and manipulate its catalytic properties. Here we report that III-nitride semiconductors have a unique ability to stabilize ultra-small ruthenium clusters (~ 0.8 nm) with high loading density up to 5 wt%. The Ru sub-nanoclusters decorated n-type III-nitride nanowires with controlled surface charge properties exhibit superior ultraviolet- and visible-light photocatalytic activity for ammonia synthesis at ambient temperature. The metal/semiconductor interfacial Schottky junction with a 0.94 eV barrier height can greatly facilitate photogenerated electron transfer from III-nitrides to Ru, making Ru act as the electron sinks which are highly beneficial to promote N≡N bond cleavage for low-temperature ammonia synthesis.

Nitrogen is one of the essential building elements for living organisms to form proteins, amino acids and nucleotides of DNA and RNA.[1] However, due to its strong nonpolar triple bond, most organisms are unable to directly metabolize molecular nitrogen (N_2), the major component of the atmosphere on earth. Therefore, nitrogen fixation by nitrogenase enzymes from certain bacteria probably ranks second only to photosynthesis as the most important biological process in nature.[2] The first artificial conversion of atmospheric nitrogen to ammonia (NH_3) was successfully achieved in the early 20th century with iron-based catalysts, the so-called the Haber-Bosch process, and is still being applied all over the world today to contribute 500+ million tons of artificial fertilizers to global agriculture per year. Besides being a fertilizer, ammonia has also gained much attention as a potential hydrogen carrier since it possesses high gravimetric hydrogen density (17.6 wt%) and is easily turned into a liquid for transportation.[3] As one of the most widely used industrial resources, the bulk market price of ammonia is highly competitive with other hydrogen storage materials (at least an order of magnitude cheaper). However, the industrial ammonia synthesis process requires high temperatures (500-600 °C) and pressures (20-50 MPa) to overcome the activation energy barrier of N_2, and consumes more than 1% of the world's annual energy supply.[4] To achieve an energy-efficient production, the development of sustainable nitrogen fixation strategy under mild conditions has become one of the greatest challenges facing us today.[5] More importantly, ammonia synthesis is an exothermic process (Eq. 1) and therefore, the equilibrium conversion will increase with decreasing temperature.

$$N_2\,(g) + 3H_2\,(g) \rightarrow 2NH_3\,(g) \quad \Delta H_{(298k)} = -92 \text{ kJ/mol} \quad \text{(Eq. 1)}$$

Similar to the natural photosynthesis process, heterogeneous photocatalytic reactions usually take place under sunlight illumination around room temperature.[6] Therefore, employing solar energy to activate inert N_2 provides an ideal approach to both access ammonia under ambient conditions without requiring extra thermal energy input and shift the equilibrium to NH_3 formation. The first photofixation of nitrogen was accomplished by Guth and Schrauzer based on a rutile-containing TiO_2 semiconductor under ultraviolet irradiation.[7] Other photoactive materials such as non-metallic buckminsterfullerene (C_{60}) molecule,[8] ultraviolet-illuminated diamond,[9] $Fe_2Ti_2O_7$,[10] Au/Nb-SrTiO$_3$,[11] and BiOBr[12] were also found capable of N_2 fixation at room temperature and atmosphere pressure.

In spite of these important features and progresses, N_2 photofixation still suffers from low efficiency due to the high-energy "N_2" intermediates (N_2^- or N_2H)[13] as well as the poor interfacial electron-transfer between the photocatalyst and adsorbed N_2. For example, most pioneering works employed semiconductor oxide powders as photocatalysts. However, the photogenerated electrons tend to recombine with their twinborn holes within a few nanoseconds, rather than to be captured by the surface adsorbed N_2 to promote the N≡N bond cleavage, which is the rate-determining step of ammonia synthesis.[14] In order to overcome these limitations, we have reasoned that well-designed nanosized semiconductors with strong electron-donating property might offer an accessible kinetic pathway toward the efficient photocatalytic N_2 fixation. Also, the incorporation of optimized Ru co-catalysts is expected to reduce the activation barrier for N_2 dissociation.[13]

Herein, we present that an efficient and stable photo-reduction of nitrogen into ammonia can be achieved by depositing ultra-small ruthenium clusters on the surfaces of GaN nanowires (NWs) with extremely high loading density (~ 10^{17} m^{-2}). While III-nitride semiconductors have been extensively utilized to fabricate electronic and optoelectronic devices, their photocatalytic activity has yet to be explored in depth.[15] Notably, the controlled *n*- and *p*-type doping, tunable band gap and the inherent chemical stability make III-group nitride a particularly suitable electronically active support for the photocatalytic ammonia synthesis reaction.

Catalyst-free gallium nitride (GaN) NWs arrays were grown directly on silicon substrate by plasma-assisted molecular beam epitaxy (MBE) under nitrogen-rich conditions (see Supporting Information). Scanning electron microscopy (SEM, Figure 1a) and transmission electron microscopy (TEM, Figure 1b) images

[*]   Dr. L. Li[+], Dr. X. Mu, Prof. C.-J. Li
       Department of Chemistry and FQRNT Center for Green Chemistry and Catalysis, McGill University, 801 Sherbrooke Street West, Montreal, QC, H3A 0B8, Canada.
       E-mail: cj.li@mcgill.ca

       Dr. L. Li[+], Dr. Y. Wang[+], S. Vanka, Prof. Z. Mi
       Department of Electrical and Computer Engineering, McGill University, 3480 University Street, Montreal, Quebec H3A 0E9, Canada.

       Prof. Z. Mi
       Department of Electrical Engineering and Computer Science, University of Michigan, 1301 Beal Avenue, Ann Arbor, MI 48109-2122, USA
       E-mail: ztmi@umich.edu

[+]   These authors contributed equally to this work.

       Supporting information for this article is given via a link at the end of the document.

of the as-synthesized GaN NWs revealed that the nanowires are about 80 nm in diameter and 800 nm in length, and are vertically aligned to the Si substrate, with the growth direction along the *c*-axis.[15b] The area density (the mass of GaN NWs per unit area) and specific surface area of the nanowires are measured to be 0.1 mg cm^{-2} and 5.7 m^2/g, respectively, which consist of 3% of the top *c*-plane and 97% of the lateral *m*-plane. Besides intrinsic GaN NWs, we have also synthesized Ge-doped n-type and Mg-doped p-type GaN NWs, since the incorporation of tetravalent (Ge^{4+}) and divalent (Mg^{2+}) ions can significantly alter the Fermi level position, surface band bending and carrier transport properties of GaN semiconductor. The electron and hole concentrations for the Ge-doped n-type and Mg-doped p-type GaN NWs were estimated to be on the order of $n = 5 \times 10^{18}$ cm^{-3} and $p = 1 \times 10^{18}$ cm^{-3}, respectively, which can be controlled by tuning the effusion cell temperatures.
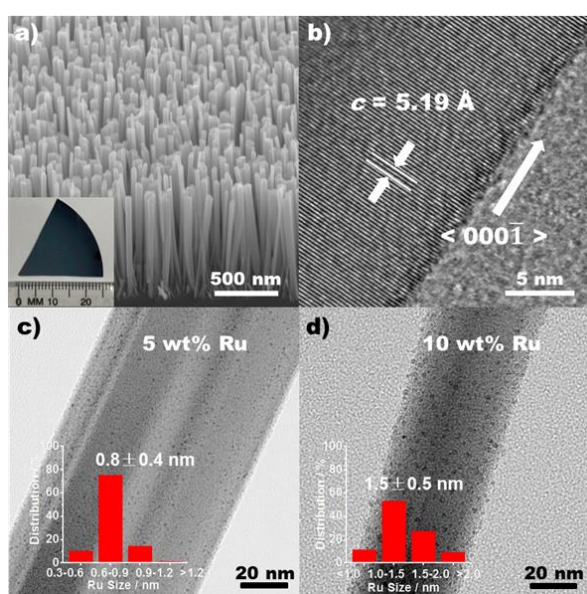

Figure 1. a) 45° tilted SEM and b) TEM images of the as-synthesized GaN NWs. The inset of a) shows the sample size. TEM images of c) 5 wt% Ru and d) 10 wt% Ru modified GaN NWs and the diameter distribution of Ru clusters (inset).

Supported ruthenium metal was introduced via the impregnation of as-synthesized GaN NWs with a solution of Ru$_3$(CO)$_{12}$ in dry THF, followed by the complete loss of carbonyl groups at elevated temperature under vacuum (Figure S1).[16] It is notable that GaN NWs exhibit unique properties to stabilize a relatively high loading of ruthenium (5 wt%) in the form of finely dispersed sub-nanoclusters with a mean diameter of 0.8 ± 0.4 nm (*average* 20 Ru/cluster, Figure 1c). Although sub-nanoclusters are usually thermodynamically unstable, these Ru clusters are firmly anchored on the surface of GaN and stable against agglomeration into large metal particles after heating at 350 °C for 2 hrs, indicating a strong interaction between Ru and the GaN lattice. The Ru species remain highly dispersed even if the loading is as high as 10 wt% (Figure 1d). The X-ray diffraction patterns (XRD, Figure S2) suggest an ideal wurtzite

crystal structure and there are no structural changes after the loading of Ru. The absence of any Ru characteristic peaks further confirms the small size of the resulting Ru clusters without any agglomeration.

The performances of GaN materials with different doping types for the photocatalytic ammonia synthesis reaction were tested at 10 °C under UV irradiation from a 300-W xenon lamp. The catalyst was placed at the bottom of an airtight quartz reactor in vacuum, followed by the introduction of a mixture of H$_2$ and N$_2$ gas (600 µmol, 75% H$_2$, 25% N$_2$). As shown in Figure 2a and Table S1, the n-type GaN NWs exhibited significantly enhanced photocatalytic activity for the NH$_3$ generation compared with the non-doped ones. On the other hand, the activity of p-type GaN NWs was slightly reduced. Besides GaN NWs, GaN powders (designated as GaN-P) also showed a substantial activity. Using a series of UV-cut-out filters, we determined that the minimum photon energy required to drive this reaction over all GaN samples corresponds to a wavelength of 360 nm. No conversion was detected under darkness. Control experiment using pure H$_2$ instead of a mixture of H$_2$ and N$_2$ revealed non-generation of NH$_3$, confirming that the NH$_3$ produced originated not from GaN decomposition, but from the photocatalytic reduction of nitrogen gas.
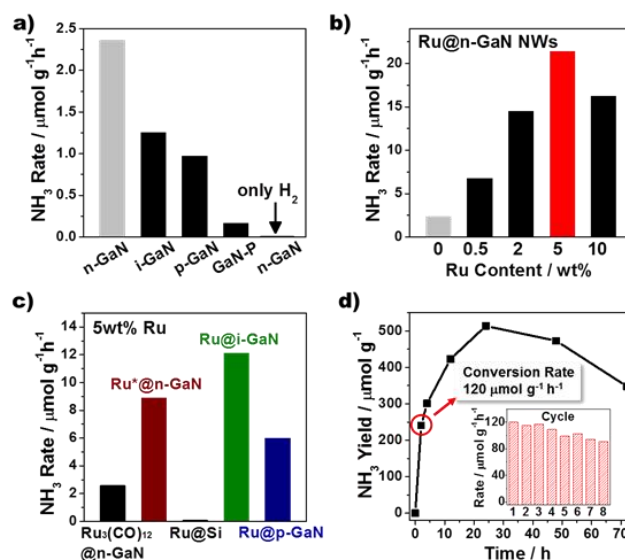

Figure 2. Ammonia generation rate over a) pure GaN materials with different doping and forms (24 h), b) Ru modified n-GaN NWs with different loading (24 h), and c) various supports with 5 wt% Ru loading (24 h). d) Plots of NH$_3$ release as a function of time over the optimized 5 wt% Ru-loaded n-GaN NWs under UV irradiation. The inset shows the reusability of Ru@n-GaN (2 h for each cycle). Reaction conditions were as follows: 0.35 mg of GaN NWs, 0.35 mg of GaN powders, and 0.35 mg of Ru@GaN upon 290-380 nm UV irradiation at an intensity of 7.5 mW cm^{-2}.

Ruthenium metal is highly efficient to promote N≡N bond cleavage by receiving electrons from the 3σ$_g$ bonding orbitals of adsorbed N$_2$ molecules and donating electrons back to the 1π$_g$* antibonding orbitals of N$_2$.[17] To further enhance the charge carrier extraction and provide more active sites for nitrogen

activation, metallic Ru co-catalysts are deposited on the GaN samples. As shown in Figure 2b, the catalytic efficiency was significantly enhanced by the introduction of Ru metal. The ammonia synthesis rate of Ru@n-GaN NWs increased with the Ru loading amount and reached a maximum at 5 wt% Ru deposition, over 9 times that of bare n-GaN NWs. When the Ru loading contents exceed 5 wt%, an obvious reduced activity was observed, which could be attributed to the decreased utilization efficiency of Ru atoms with the increasing cluster size.

To gain a better understanding of the nature of the catalytic active sites, Ru modified n-GaN NWs through the decomposition of RuCl$_3$ precursor (designated as Ru*@n-GaN) and Ru$_3$(CO)$_{12}$ modified n-GaN NWs have been prepared, respectively. It is found that the incorporation of Ru$_3$(CO)$_{12}$ has negligible effect on the catalytic activity compared to the bare n-GaN NWs (Figure 2c), likely because Ru atoms in Ru$_3$(CO)$_{12}$ are coordinatively saturated and thus unavailable for N$_2$ insertion. On the other hand, although the content, shape, and size of Ru species in Ru*@n-GaN are similar to those in Ru@n-GaN, as confirmed by TEM, XRD and X-ray photoelectron spectroscopy (XPS), the photoactivity of Ru*@n-GaN, however, was much lower than that of Ru@n-GaN under the same reaction conditions (Figure 2c). This phenomenon implies that the remained chlorine ions located on the ruthenium metal surface can act as a poison against ammonia synthesis since the active sites available for hydrogen chemisorption will be inhibited by chlorine ions.[18] Consequently, our results show that the ruthenium co-catalyst is quite sensitive and employing Cl-free Ru precursors is highly critical to achieve the best catalytic performances.

The electronic property of the semiconductor has a fundamental influence on the catalytic activity of supported metal species.[6c,19] As shown in Figures 2b and 2c, the NH$_3$ generation rate of Ru@n-GaN is significantly higher than Ru@p-GaN. An average NH$_3$ generation rate of 120 μmol h^{-1} g^{-1} was achieved after 2-h UV irradiation by using 0.35 mg of the optimized Ru@n-GaN NWs with 5 wt% Ru (Figure 2d) at 10 °C, corresponding to 2400 umol h^{-1} g^{-1} based on Ru (TOF = 0.24 h^{-1}). Compared with previously published results,[20] the activity of Ru@n-GaN is enhanced by a factor of 5 under similar conditions around room temperature. The ammonia concentration reached a maximum after 24-h of irradiation and decreased gradually with prolonging the reaction time, since a further decomposition of NH$_3$ became dramatic if the produced NH$_3$ was not removed from the reactor promptly. The reusability of Ru@n-GaN for ammonia synthesis was tested (inset of Figure 2d) and the catalytic results showed that the Ru@n-GaN catalyst can be used repeatedly after eight catalytic runs with slight deactivation. The crystal structure and morphology of the catalyst sample remained intact after reaction run for a long time, as judged by the XRD, SEM and TEM (Figure S3). The control experiment has shown that the reaction does not proceed at all in the absence of GaN matrix (exemplified by using pure Si wafer as support).

In the case of Ru@n-GaN, the electron will flow from n-GaN NWs into Ru sub-nanoclusters on contact since the Fermi level of n-GaN NWs is above that of Ru metal (Figure 3a). Consequently, a depletion layer will be established at the

interface, where the Ru metal is negatively charged and the semiconductor is positively charged near the surface (Figure S4a). The influence of this electrostatic induction could spread throughout the whole Ru clusters due to its ultra-small size less than 1 nm. On the other hand, a reduction of local electron density at Ru cluster will be induced by the opposite electric field in Ru@p-GaN (Figure S4b). The XPS results clearly indicated that the Ru 3d peaks of Ru@n-GaN are negatively shifted (285.2 eV) compared to the binding energies of Ru on i-GaN (285.5 eV) and p-GaN (285.8 eV), respectively (Figure 3b). These results suggest that n-type GaN NWs could function as an efficient electron donor to produce Ru species with high electron density, which can act as Lewis base sites and are highly beneficial to the reduction of nitrogen.
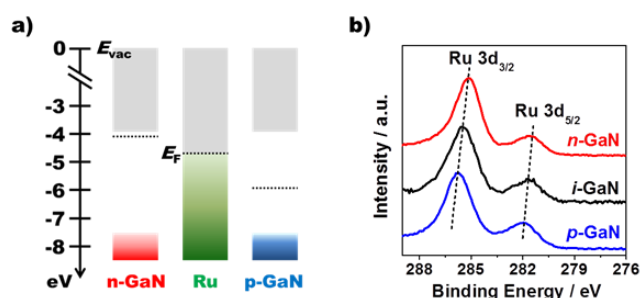

Figure 3. a) Comparison of the energy band diagram and Fermi level (E_F) in n-type GaN NWs, Ru metal and p-type GaN NWs. E_{vac} denotes vacuum level. b) XPS spectra of Ru 3d for the different Ru modified catalysts.

Since the work function of Ru metal (Φ_M = 4.7 eV) is higher than that of n-type GaN semiconductor (Φ_S = 4.1 eV),[21] a resulting upward band bending will be formed at the interface to create a potential barrier, known as the Schottky barrier.[22] As illustrated in Figure 4a, the formed Schottky barrier can serve as irreversible electron sink to trap the photo-induced electrons from n-GaN NWs under photoexcitation, which can remarkably prevent electron-hole recombination and often results in an enhanced photocatalytic performance. Based on the Schottky-Mott theory, the barrier height (Φ_{SB}) follows the rule ($\Phi_{SB} = \Phi_M - \chi_S$), where χ_S is electron affinity of n-GaN NWs. However, in case of low dimensional systems, Schottky barrier height depends not only on the work functions, but also on the annealing temperature, image-force effect, and the existence of Fermi level pinning by surface states.[23] To determine the barrier height value (Φ_{SB}) of Ru sub-nanoclusters on n-GaN NWs, a series of XPS spectra were measured according to Eq. 2.[24]

$$\Phi_{SB} = E_g - (E_F - E_V^i) + (E_{CL}^i - E_{CL}^m) \quad \text{(Eq. 2)}$$

E_g (3.4 eV) is the band gap of n-GaN NWs, E_F is the Fermi level, E_V^i is the initial binding energy of the valence band maximum of the fresh n-GaN NWs, E_{CL}^i is the initial binding energy of the fresh n-GaN NWs core level peak and E_{CL}^m is the binding energy of the n-GaN NWs core level peak after metal deposition. All binding energies are measured relative to the Fermi energy (E_F = 0 eV). As shown in Figure 4b, the near-surface $E_F - E_V^i$ of the intact n-GaN NWs was measured to be 3.35 eV, which decreased distinctly following the Ru deposition, indicating an

increase in upward band bending. The precise determination of Φ_{SB} will be calculated based on the differences in Ga 3d core level energies. Figure 4c demonstrated clearly that there exists a core-level shift of 0.89 eV ($E^i_{CL} - E^m_{CL}$) towards the lower binding energy with Ru deposition. Consequently, the Schottky barrier height Φ_{SB} are calculated to be 0.94 eV, according to Eq. 2.

Figure 4d shows the room-temperature photoluminescence (PL) spectrum of n-GaN NWs before and after the Ru deposition. Although the PL bands are both located at ca. 365 nm, corresponding to the GaN band gap of 3.4 eV, the peak intensity of Ru@n-GaN is much weaker than that of pure n-GaN under the same measurement conditions. The reduction in PL intensity after the Ru deposition further demonstrated that the formed Schottky barrier can act as electron trappers to improve photogenerated electron-hole separation.
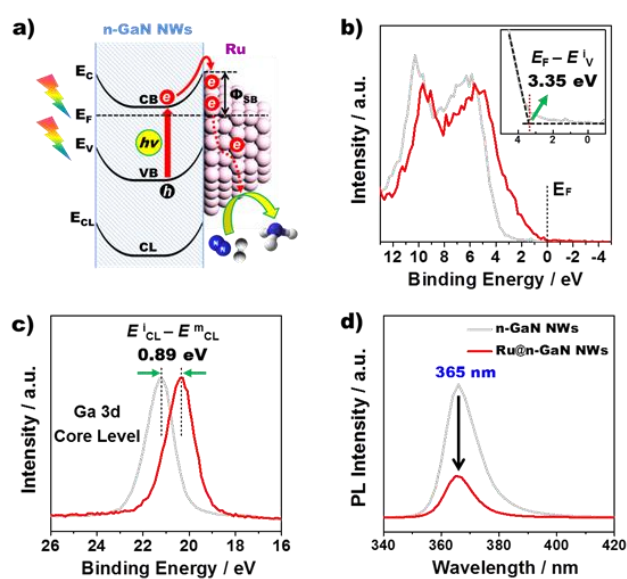
further doped with Ge^{4+} or Mg^{2+} ions as n-type or p-type dopants, respectively. The room temperature PL spectrum (Figure 5c) of InGaN/GaN nanowires clearly shows a single band-to-band optical emission peak at ca. 531 nm, corresponding to an InGaN band gap of 2.34 eV with an average In composition of ca. 25%.[27] Figure 5d gave the photocatalytic results of various InGaN/GaN samples for ammonia synthesis under visible light irradiation (> 400 nm) at room temperature. Compared with the p-type and intrinsic samples, n-InGaN/n-GaN nanowire arrays exhibit the highest activity (designated as n-InGaN), which could be further improved by the deposition of 5 wt% Ru (Figure S6). In contrast, pure n-GaN sample without indium incorporation did not show any activity under the same conditions.
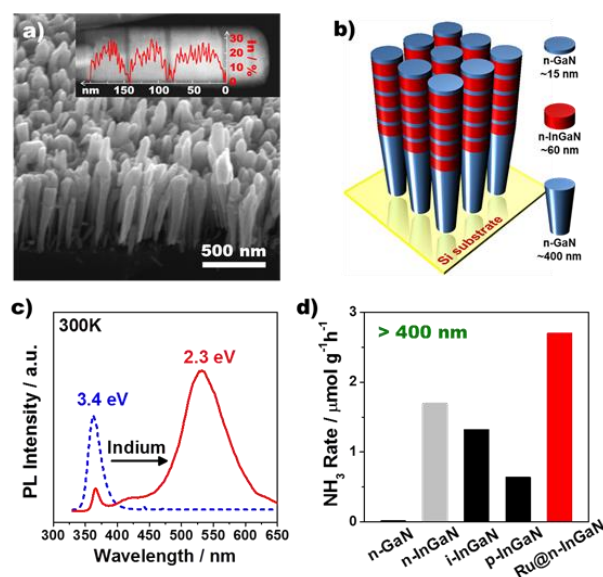

Figure 4. a) Schematic diagram for the formation of the Schottky barrier between n-type GaN NWs and metallic Ru clusters. b) XPS valence band spectra, c) Ga 3d core level XPS spectra, and d) PL spectra of n-GaN NWs before (gray curve) and after the deposition of Ru (red curve). The Inset of b) illustrates the near Fermi level (E_F) region and valence band maximum position $E_F - E^i_V$ of pure n-GaN NWs.

Figure 5. a) A 45 °C tilted SEM image of as-grown InGaN/GaN nanowires on Si (111) substrate. The inset shows STEM-HAADF image of a single InGaN/GaN nanowire and a line-profile analysis for the distribution of In content. b) Schematic of InGaN/GaN nanowire structure showing five InGaN nanowire segments on a GaN nanowire template. c) Room temperature PL spectrum from as-synthesized InGaN/GaN nanowires. d) Ammonia generation rate over various III-nitride materials under visible-light irradiation. Reaction conditions were as follows: 0.35 mg of III-nitride and 5 wt% Ru@InGaN/GaN NWs upon visible-light irradiation at an intensity of 20 mW cm^{-2} for 24 h.

The band gap of GaN can shift from UV to visible region by incorporating indium element.[15c] To further realize visible-light photoactivity of III-nitrides towards ammonia synthesis, we have designed and synthesized an InGaN/GaN nanowire arrays on Si (111) substrate by MBE (Figure 5a).[25] Detailed structure and elemental distribution were characterized using high-angle annular dark-field (HAADF)/scanning transmission electron microscopy (STEM) and energy-dispersive X-ray scanning (EDXS) analysis (the inset of Figure 5a), revealing the existence of the segment structure and the distribution of the indium components in the nanowires. As illustrated in Figures 5b and S5,[26] five segments of InGaN ternary wires were incorporated along the growth direction of GaN nanowire to suppress indium phase separation. The height of each InGaN/GaN segment was controlled by the growth time (~ 2.5 nm/min), which could be

In summary, a promising photo-induced approach to access ammonia synthesis at ambient conditions has been realized over Ru-supported III-nitride hybrids. The GaN nanowires exhibit superior ability to stabilize ultra-small Ru sub-nanoclusters with high loading density. The catalytic activity of the loaded Ru is very sensitive to its electronic property, Cl-free precursor and support. We have demonstrated that Ge^{4+} doped n-type GaN NWs could act as an efficient electron donor for the Ru co-catalyst, forming Schottky barrier junction and resulting in partially negatively charged Ru species with an enhanced catalytic performance. The visible-light photoactivity for ammonia synthesis could be further achieved by the incorporation of indium element into GaN NWs.

Experimental Section

The deposition of Ru co-catalyst. Ruthenium loading was conducted via the impregnation of as-synthesized GaN NWs (0.35 mg) with a solution of $Ru_3(CO)_{12}$ in dry THF (1.5 mL), followed by the complete loss of carbonyl groups in vacuum under a temperature program of 2 ^oC min^{-1} up to 200 ^oC, held for one hour, 1 ^oC min^{-1} up to 350 ^oC, held for two hours and then cooled to ambient temperature. The Ru content was further confirmed by using the XPS measurement before and after the decomposition process.

Photo-driven ammonia synthesis. A slice of freshly prepared GaN or InGaN/GaN NWs with areas of 3.5 cm^2 (corresponding to 0.35 mg of GaN NWs) was placed on the bottom of an air-tight quartz reactor in vacuum, followed by the introduction of 600 μmol hydrogen (75 %) and nitrogen (25 %) mixture (Figure S7). In the case of powdered samples, 0.35 mg of powders was spread evenly on the bottom of the reactor in vacuum, which was then evacuated at 250 ^oC for 2 h to remove water and other molecules adsorbed in the powders. The light intensity measured at wavelengths between 290 and 380 nm was ca. 7.5 $mWcm^{-2}$. The light intensity measured at wavelengths longer than 400 nm was ca. 20 $mWcm^{-2}$. The NH_3 product was identified by gas chromatography-mass spectrometry and quantified via a colorimetric method. Specifically, 1.5 mL of deionized water was injected into the chamber to fully dissolve the NH_3 (gas phase) formed after the reaction. Then, 80 μL of an aqueous solution of EDTA tetrasodium salt hydrate (1.3 M), 160 μL of an aqueous solution of sodium salicylate (1.46 M) and pyrazole (0.24 M), 520 μL of an aqueous solution of sodium hydroxide (1.25 M) and sodium hypochlorite (0.25 M) were added consequently. In the presence of NH_3, a green color complex with absorption at 650 nm was measured by UV/vis spectrometer (Figure S8). Ammonium chloride was employed for making the calibration curve (Figure S9).

Characterization. The powder X-ray diffraction (XRD) patterns were recorded on a Bruker D8 Advanced Diffractometer with Cu Kα radiation (λ = 1.5418 Å). Scanning electron microscopy (SEM) images were recorded using LASEM Hitachi S-4700. High resolution bright field transmission electron microscope (TEM) images were obtained using FEI Tecnai G2 F20 S/TEM at accelerating voltage of 200 kV. For STEM-HAADF imaging, a Hitachi HD2700 Cs-corrected STEM was used with a cold field emitter operated at 200 kV and with an electron beam diameter of ~ 0.1 nm. STEM EDXS analysis was performed using a 60 mm^2 silicon drift detector from Bruker. The UV-vis absorption spectra were measured with a Shimadzu UV-2450 spectrophotometer. The X-ray photoelectron spectroscopy (XPS) was performed on an ESCALAB 250 X-ray photoelectron spectrometer with a monochromated X-ray source (Al Kα $h\upsilon$ = 1486.6 eV). The energy scale of the spectrometer was calibrated using Au $4f_{7/2}$, Cu $2p_{3/2}$, and Ag $3d_{5/2}$ peak positions. The standard deviation for the binding energy (BE) values was 0.1 eV. The E_F - E_V was estimated for each sample from XPS valence band spectrum. The PL measurement was performed with either a 405-nm laser or a 325-nm He-Cd laser (Kimmon Koha) as excitation source. The laser beam was focused on the sample through a × 60 objective, with a circular beam size of ~ 5 μm. The emitted light was collected by the same objective and spectrally resolved by a high-resolution spectrometer and detected by a photomultiplier tube.

Acknowledgements

[1]   I. Coric, B. Q. Mercado, E. Bill, D. J. Vinyard, P. L. Holland, *Nature* **2015**, *526*, 96-99.

[2]   B. E. Smith, *Science* **2002**, *297*, 1654-1655.

[3]   W. Zheng, T. P. Cotter, P. Kaghazchi, T. Jacob, B. Frank, K. Schlichte, W. Zhang, D. S. Su, F. Schüth, R. Schlögl, *J. Am. Chem. Soc.* **2013**, *135*, 3458-3464.

[4]   J. W. Erisman, M. A. Sutton, J. Galloway, Z. Klimont, W. Winiwarter, *Nat. Geosci.* **2008**, *1*, 636-639.

[5]   Y. Nishibayashi, *Inorg. Chem.* **2015**, *54*, 9234-9247.

[6]   a) L. Li, G.-D. Li, C. Yan, X.-Y. Mu, X.-L. Pan, X.-X. Zou, K.-X. Wang, J.-S. Chen, *Angew. Chem. Int. Ed.* **2011**, *50*, 8299-8303; b) L. Li, Y.-Y. Cai, G.-D. Li, X.-Y. Mu, K.-X. Wang, J.-S. Chen, *Angew. Chem. Int. Ed.* **2012**, *51*, 4702-4706; c) L. Li, X. Mu, W. Liu, Z. Mi, C. J. Li, *J. Am. Chem. Soc.* **2015**, *137*, 7576-7579.

[7]   G. N. Schrauzer, T. D. Guth, *J. Am. Chem. Soc.* **1977**, *99*, 7189-7193.

[8]   Y. Nishibayashi, M. Saito, S. Uemura, S.-i. Takekuma, H. Takekuma, Z.-i. Yoshida, *Nature* **2004**, *428*, 279-280.

[9]   D. Zhu, L. Zhang, R. E. Ruther, R. J. Hamers, *Nat. Mater.* **2013**, *12*, 836-841.

[10]   O. Rusina, A. Eremenko, G. Frank, H. P. Strunk, H. Kisch, *Angew. Chem. Int. Ed.* **2001**, *40*, 3993-3995.

[11]   T. Oshikiri, K. Ueno, H. Misawa, *Angew. Chem. Int. Ed.* **2014**, *53*, 9802-9805.

[12]   H. Li, J. Shang, Z. Ai, L. Zhang, *J. Am. Chem. Soc.* **2015**, *137*, 6393-6399.

[13]   K. Honkala, A. Hellman, I. N. Remediakis, A. Logadottir, A. Carlsson, S. Dahl, C. H. Christensen, J. K. Nørskov, *Science* **2005**, *307*, 555-558.

[14]   M. Kitano, Y. Inoue, Y. Yamazaki, F. Hayashi, S. Kanbara, S. Matsuishi, T. Yokoyama, S.-W. Kim, M. Hara, H. Hosono, *Nat. Chem.* **2012**, *4*, 934-940.

[15]   a) D. Wang, A. Pierre, M. G. Kibria, K. Cui, X. Han, K. H. Bevan, H. Guo, S. Paradis, A.-R. Hakima, Z. Mi, *Nano Lett.* **2011**, *11*, 2353-2357; b) L. Li, S. Fan, X. Mu, Z. Mi, C.-J. Li, *J. Am. Chem. Soc.* **2014**, *136*, 7793-7796; c) M. G. Kibria, F. A. Chowdhury, S. Zhao, B. AlOtaibi, M. L. Trudeau, H. Guo, Z. Mi, *Nat. Commun.* **2015**, *6*, 6797.

[16]   D. K. Chakrabarty, A. Joshi, S. Unnikrishnan, P. D. Prabhawalkar, *React. Kinet. Catal. L.* **1984**, *26*, 143-147.

[17]   C. N. R. Rao, G. Ranga Rao, *Surf. Sci. Rep.* **1991**, *13*, 223-263.

[18]   a) S. Murata, K.-I. Aika, *Appl. Catal. A: Gen.* **1992**, *82*, 1-12; b) K. Lu, B. J. Tatarchuk, *J. Catal.* **1987**, *106*, 166-175.

[19]   S. Schäfer, S. A. Wyrzgol, R. Caterino, A. Jentys, S. J. Schoell, M. Hävecker, A. Knop-Gericke, J. A. Lercher, I. D. Sharp, M. Stutzmann, *J. Am. Chem. Soc.* **2012**, *134*, 12528-12535.

[20]   H. Zeng, S. Terazono, T. Tanuma, *Catal. Commun.* **2015**, *59*, 40-44.

[21]   J. S. Foresi, T. D. Moustakas, *Appl. Phys. Lett.* **1993**, *62*, 2859-2861.

[22]   Z. Zhang, J. T. Yates, *Chem. Rev.* **2012**, *112*, 5520-5551.

[23]   S. M. Sze, K. K. Ng, *Physics of Semiconductor Devices, 3rd Edition*, John Wiley & Sons, New York, **2007**.

[24]   a) E. A. Kraut, R. W. Grant, J. R. Waldrop, S. P. Kowalczyk, *Phys. Rev. Lett.* **1980**, *44*, 1620-1623; b) J. R. Waldrop, R. W. Grant, *Appl. Phys. Lett.* **1988**, *52*, 1794-1796; c) K. M. Tracy, P. J. Hartlieb, S. Einfeldt, R. F. Davis, E. H. Hurt, R. J. Nemanich, *J. Appl. Phys.* **2003**, *94*, 3939-3948.

[25]   B. AlOtaibi, X. Kong, S. Vanka, S. Y. Woo, A. Pofelski, F. Oudjedi, S. Fan, M. G. Kibria, G. A. Botton, W. Ji, H. Guo, Z. Mi, *ACS Energy Lett.* **2016**, *1*, 246-252.

[26]   H. P. T. Nguyen, S. Zhang, K. Cui, X. Han, S. Fathololoumi, M. Couillard, G. A. Botton, Z. Mi, *Nano Lett.* **2011**, *11*, 1919-1924.

[27]   P. G. Moses, C. G. V. d. Walle, *Appl. Phys. Lett.* **2010**, *96*, 021908.

COMMUNICATION

III-nitride semiconductors have a unique ability to stabilize ultra-small ruthenium clusters with high loading density up to 5 wt%. The metal/semiconductor interfacial Schottky junction can greatly facilitate photogenerated electron transfer from III-nitrides to Ru, making Ru act as the electron sinks which are highly beneficial to promote N≡N bond cleavage for low-temperature ammonia synthesis.
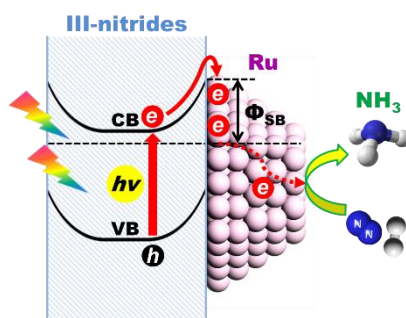
Lu Li, Yichen Wang, Srinivas Vanka, Xiaoyue Mu, Zetian Mi* and Chao-Jun Li*

Page No.1 – Page No.5

Nitrogen Photofixation over III-Nitride Nanowires Assisted by Ruthenium Clusters of Low Atomicity

Author Manuscript

Supporting Information

Nitrogen Photofixation over III-Nitride Nanowires Assisted by Ruthenium Clusters of Low Atomicity

Lu Li,[1,2] Yichen Wang,[2] Srinivas Vanka,[2] Xiaoyue Mu,[1] Zetian Mi[*2,3] and Chao-Jun Li[*1]

[1]Department of Chemistry and FQRNT Center for Green Chemistry and Catalysis, McGill University, 801 Sherbrooke Street West, Montreal, QC, H3A 0B8, Canada.

[2]Department of Electrical and Computer Engineering, McGill University, 3480 University Street, Montreal, Quebec H3A 0E9, Canada.

[3]Department of Electrical Engineering and Computer Science, University of Michigan, 1301 Beal Avenue, Ann Arbor, MI 48109-2122, USA.

cj.li@mcgill.ca

ztmi@umich.edu

1

1. Growth of GaN and InGaN/GaN Nanowires.

The catalyst-free GaN and InGaN/GaN nanowires are grown on a Si (111) substrate using radio frequency plasma-assisted molecular beam epitaxy (MBE) in nitrogen rich conditions. Prior to loading into the MBE system, the Si substrates were cleaned by hydrofluoric acid and standard solvent solutions. Growth conditions include the following: a temperature of ~750 °C, nitrogen flow rate of 1 sccm, and a forward plasma power of ~400 W. The as-synthesized nanowires can be doped with tetravalent (Ge^{4+}) and divalent (Mg^{2+}) ions to make it n and p type, respectively. The doping density is controlled by tuning the effusion cell temperatures of Ge, Mg and In. For n-type doping, the Ge effusion cell temperature is 1100 °C. For p-type doping, the Mg effusion cell temperature is 265 °C. For the incorporation of indium, the indium effusion cell temperature is varied from 705 °C to 795 °C. The electron and hole concentrations for the Si-doped n-type and Mg-doped p-type GaN NWs were estimated to be on the order of $n = 5 \times 10^{18}$ cm^{-3} and $p = 1 \times 10^{18}$ cm^{-3}, respectively. Other growth parameters were kept constant.

2. The deposition of Ru co-catalyst.

Ruthenium loading was conducted via the impregnation of as-synthesized GaN NWs (0.35 mg) with a solution of $Ru_3(CO)_{12}$ in dry THF (1.5 mL), followed by the complete loss of carbonyl groups in vacuum under a temperature program of 2 °C min^{-1} up to 200 °C, held for one hour, 1 °C min^{-1} up to 350 °C, held for two hours and then cooled to ambient temperature.

3. Photo-driven ammonia synthesis.

A slice of freshly prepared GaN or InGaN/GaN NWs with areas of 3.5 cm^2 (corresponding to 0.35 mg of GaN NWs) was placed on the bottom of an air-tight quartz reactor in vacuum, followed by the introduction of 600 μmol hydrogen (75 %) and nitrogen (25 %) mixture. In the case of powdered samples, 0.35 mg of powders was spread evenly on the bottom of the reactor in vacuum, which was then evacuated at 250

^{o}C for 2 h to remove water and other molecules adsorbed in the powders. The light intensity measured at wavelengths between 290 and 380 nm was ca. 7.5 mWcm^{-2}. The light intensity measured at wavelengths longer than 400 nm was ca. 20 mWcm^{-2}. The NH$_3$ product was qualitatively analyzed by gas chromatography-mass spectrometry and quantitatively determined via a colorimetric method.

4. Quantitative determination of NH$_3$

The quantitative determination of NH$_3$ was using a colorimetric method.

(1) 1.5 mL of deionized water was injected into the chamber to fully dissolve the NH$_3$ (gas phase) formed after the reaction (deginated as solution A).

(2) 80 μL of an aqueous solution of EDTA tetrasodium salt hydrate (1.3 M) was added into solution A.

(3) 160 μL of an aqueous solution of sodium salicylate (1.46 M) and pyrazole (0.24 M) added into solution A.

(4) 520 μL of an aqueous solution of sodium hydroxide (1.25 M) and sodium hypochlorite (0.25 M) were added into solution A.

In the presence of NH$_3$, a green color complex with absorption at 650 nm was measured by UV/vis spectrometer (Figure S8). A series of ammonium chloride with known concentration were employed for making the calibration curve (Figure S9).

5. Generation Characterization.

The powder X-ray diffraction (XRD) patterns were recorded on a Bruker D8 Advanced Diffractometer with Cu Kα radiation (λ = 1.5418 Å). Scanning electron microscopy (SEM) images were recorded using LASEM Hitachi S-4700. High resolution bright field transmission electron microscope (TEM) images were obtained using FEI Tecnai G2 F20 S/TEM at accelerating voltage of 200 kV. For STEM-HAADF imaging, a Hitachi HD2700 Cs-corrected STEM was used with a cold field emitter operated at 200 kV and with an electron beam diameter of ~ 0.1 nm. STEM EDXS analysis was performed using a 60mm^2 silicon drift detector from Bruker. The UV-vis absorption spectra were measured with a Shimadzu UV-2450 spectrophotometer. The X-ray photoelectron spectroscopy (XPS) was performed on an ESCALAB 250 X-ray

3

photoelectron spectrometer with a monochromated X-ray source (Al Kα $h\upsilon$ = 1486.6 eV). The energy scale of the spectrometer was calibrated using Au $4f_{7/2}$, Cu $2p_{3/2}$, and Ag $3d_{5/2}$ peak positions. The standard deviation for the binding energy (BE) values was 0.1 eV. The E_F - E_V was estimated for each sample from XPS valence band spectrum. The PL measurement was performed with either a 405-nm laser or a 325-nm He-Cd laser (Kimmon Koha) as excitation source. The laser beam was focused on the sample through a × 60 objective, with a circular beam size of ~ 5 μm. The emitted light was collected by the same objective and spectrally resolved by a high-resolution spectrometer and detected by a photomultiplier tube.

4

Figure S1. EDX spectrum of 5 wt% Ru modified GaN NWs.
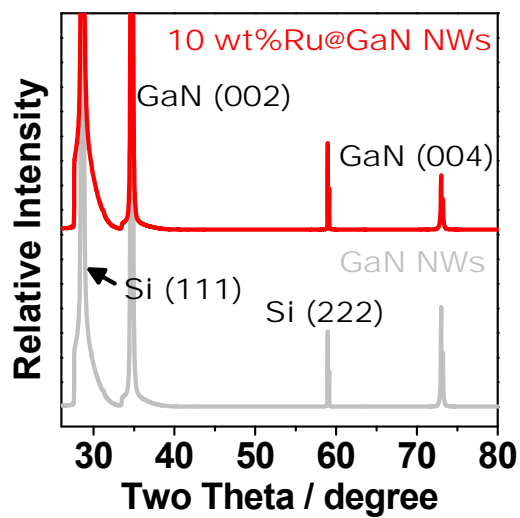
Figure S2. XRD patterns of GaN nanowires before (gray) and after (red) the deposition of Ru metal.
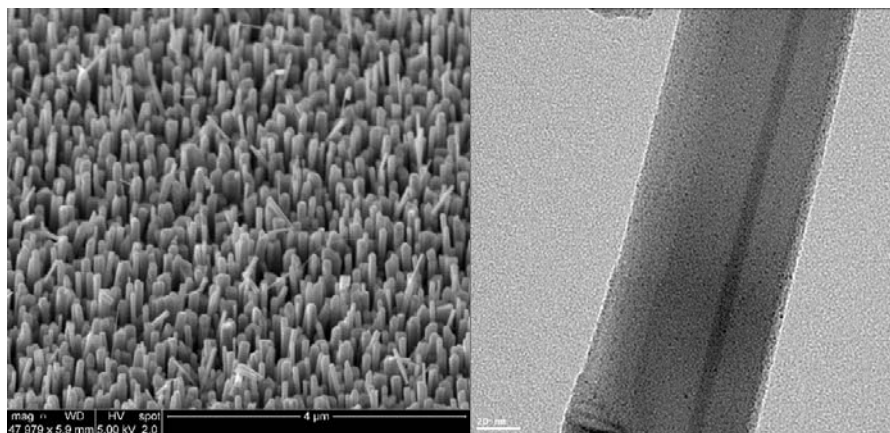
Figure S3. SEM (left) and TEM (right) images of the Ru@GaN NWs after 24h of photocatalytic reaction.
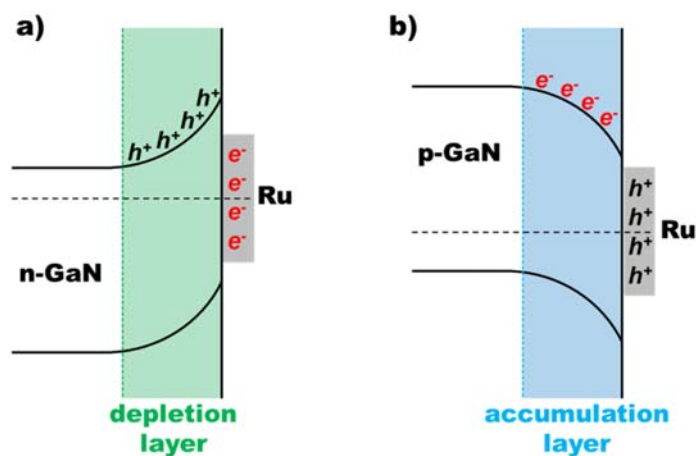

Figure S4. Energy band diagrams of Ru metal and GaN semiconductor contacts. (a) The formation of depletion layer between Ru and n-GaN NWs. (b) The formation of accumulation layer between Ru and p-GaN NWs.
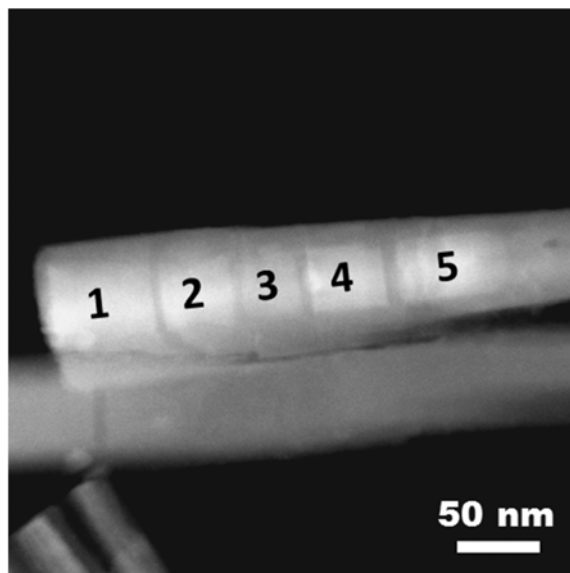
6

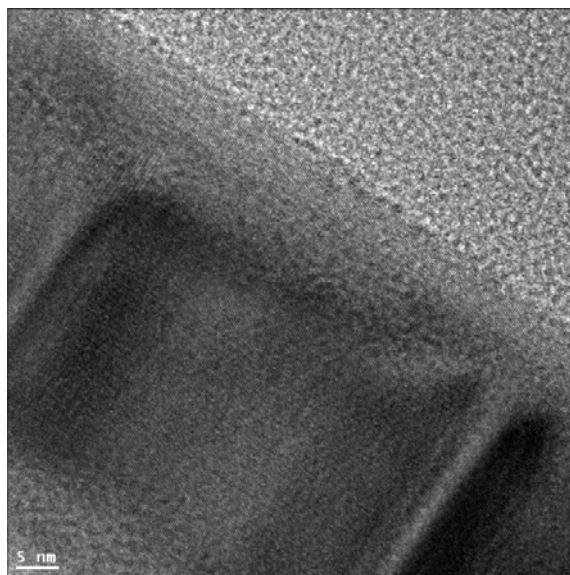**Figure S5.** STEM-HAADF image of the as-synthesized InGaN/GaN NWs with five InGaN segments.

Figure S6. TEM image of 5 wt % Ru modified InGaN/GaN NWs.

7

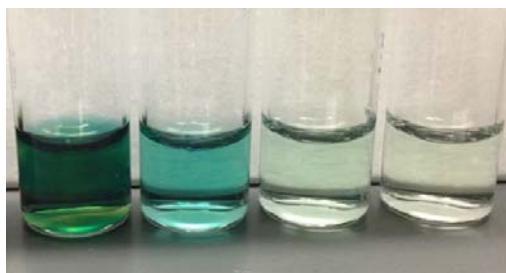**Figure S7.** Reaction setup.

Figure S8. Photos of green complex obtained during the ammonia synthesis reaction, after performing the colorimetric treatment.
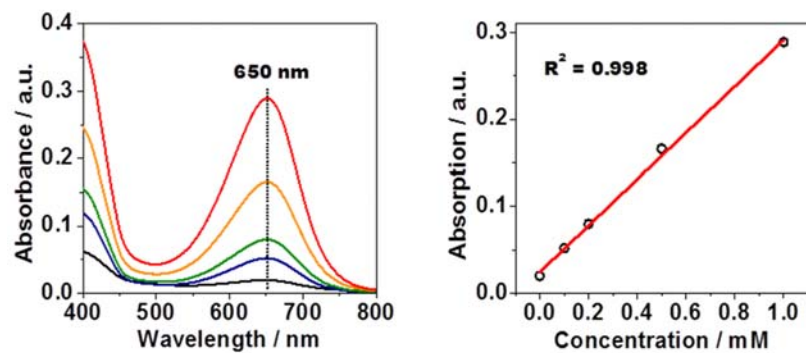
8

Figure S9. UV-vis spectroscopy calibration data for the quantitative determination of NH$_3$ at maximum absorbance peak of 650 nm (left) and the calibration curve (right).

Table S1. Results of various samples for the photocatalytic ammonia synthesis.[a]

Entry	Substrates	Time (h)	Wavelength (nm)	NH₃ yield (μmol/g)
1	i-GaN NWs	24	> 290 nm	30
2	n-GaN NWs	24	> 290 nm	57
3	p-GaN NWs	24	> 290 nm	23
4	GaN powder	24	> 290 nm	4
5	0.5 wt%Ru@n-GaN NWs	24	> 290 nm	162
6	2 wt%Ru@n-GaN NWs	24	> 290 nm	348
7	5 wt%Ru@n-GaN NWs	24	> 290 nm	514
8	10 wt%Ru@n-GaN NWs	24	> 290 nm	390
9	5 wt%Ru@n-GaN NWs	24	Dark	n.d.
10	5 wt%Ru@n-GaN NWs	2	> 290 nm	241
11	5 wt%Ru@n-GaN NWs	4	> 290 nm	301
12	5 wt%Ru@n-GaN NWs	12	> 290 nm	423
13	5 wt%Ru@n-GaN NWs	48	> 290 nm	473
14	5 wt%Ru@n-GaN NWs	72	> 290 nm	348
15	5 wt%Ru$_3$(CO)$_{12}$@n-GaN NWs	24	> 290 nm	62
16	5 wt%Ru*@n-GaN NWs	24	> 290 nm	213
17	5 wt%Ru@i-GaN NWs	24	> 290 nm	291
18	5 wt%Ru@p-GaN NWs	24	> 290 nm	144
19	5 wt%Ru@Si substrate	24	> 290 nm	trace
20	n-InGaN/n-GaN NWs	24	> 400 nm	41
21	i-InGaN/i-GaN NWs	24	> 400 nm	32
22	p-InGaN/p-GaN NWs	24	> 400 nm	15
23	5 wt%Ru@n-InGaN/n-GaN NWs	24	> 400 nm	65
24	n-GaN NWs	24	> 400 nm	n.d.[b]
25	5 wt%Ru@n-GaN NWs	24	> 400 nm	n.d.

[a]Reaction conditions were as follows: reaction temperature, 10 °C; reactant, 600 μmol of H_2 (75%) and N_2 (25%); irradiation source, 290-380 nm UV irradiation at an intensity of 7.5 mWcm^{-2}; irradiation time, 2-72 h. After the reaction. [b]Not detectable

10